Control of ion energy distribution in low-pressure and triple-frequency capacitive discharge

2009 Plasma Sources Sci. Technol. 18 025024

(http://iopscience.iop.org/0963-0252/18/2/025024)

Plasma Sources Sci. Technol. **18** (2009) 025024 (9pp) doi:10.1088/0963-0252/18/2/025024

Control of ion energy distribution in low-pressure and triple-frequency capacitive discharge

S H Lee, Pawan K Tiwari, J K Lee

Department of Electronic and Electrical Engineering, Pohang University of Science and Technology, Pohang 790-784, Korea

E-mail: jkl@postech.ac.kr

Received 10 June 2008, in final form 21 September 2008
Published 31 March 2009
Online at stacks.iop.org/PSST/18/025024

Abstract

One-dimensional particle-in-cell Monte Carlo collision (PIC-MCC) simulations of low-pressure (10 mTorr) argon plasmas sustained by a triple-frequency (1, 30 and 120 MHz) source in symmetrical current-driven and voltage-driven capacitively coupled plasma reactors are carried out. We concluded that the effective current, the effective voltage and the effective frequency are helpful in explaining the physics of triple-frequency capacitively coupled plasma sources (CCPs) alike single-frequency CCPs. The rf discharge parameters such as the ion energy distribution function (IEDF), the sheath length, the plasma potential and the powers dissipated by electrons and ions can be expressed as the effective frequency and the effective current density (or effective voltage). The analytical model of the IEDF for triple-frequency CCPs in the high-frequency regime is developed. The analytical calculations of the IEDF in the high-frequency regime through the effective frequency visualized in this paper are compared with the simulation results of the IEDF calculated from the 1D PIC-MCC model. The ion energy width and the average ion energy of the IEDF are controlled by the effective frequency, which is expressed as a function of the current density (or voltage) and frequency ratios of the triple-frequency source. The evolution of the effective frequency with the current density or voltage ratio of three frequency sources is different depending on the mode of operating source, which is either voltage or current. The effective frequency in voltage-driven CCPs is 2–10 times higher than that of current-driven CCPs at the same ratio of current density and voltage. As a result, the current-driven CCPs is more desirable than the voltage-driven CCPs from the aspect of independent control of ion flux and ion bombardment energy because the ion energy width increases with decreasing effective frequency.

(Some figures in this article are in colour only in the electronic version)

1. Introduction

Conventional capacitively coupled plasma sources (CCPs) with a single frequency of 13.56 MHz were widely used for dielectric etching, deposition and surface treatment processes in the semiconductor industry. The technology of the dielectric etching process that demands for a deep trench with a high aspect ratio requires improvement in conventional CCPs. Therefore, dual-frequency CCPs, that can independently control the ion flux and the ion energy distribution, have been effectively used for the etching process. There have been a large number of analytical and numerical investigations for the physics of ion energy distribution function (IEDFs) in single-frequency and dual-frequency CCPs.

The analytical model of IEDFs in a single-frequency capacitive collisionless rf sheath gives only the qualitative features of IEDFs due to the approximations such as the constant sheath width and the sinusoidal sheath potential drop [1–3]. The IEDFs on the driven electrode are affected by the ratio of the ion transit time (τ_{ion}) to the rf period

(τ_{rf}), which is expressed as functions of the rf frequency, the sheath length and the mean potential difference between the driven electrode and the plasma [1, 4–6]. When $\tau_{ion}/\tau_{rf} \leqslant 1$, ions respond to the instantaneous sheath voltage. When $\tau_{ion}/\tau_{rf} \gg 1$, ions respond to the average sheath voltage because ions cross the sheath in a time corresponding to many rf cycles. Georgieva *et al* suggested the analytical model of IEDFs in a collisionless sheath for dual-frequency CCPs, and their analytical results are in good agreement with particle-in-cell Monte Carlo collision (PIC-MCC) simulation results [7]. They observed that the ion energy width increases by adding the low-frequency (1 or 2 MHz) source to the high-frequency (27 MHz) source, and the ion energy width for the low-frequency (1 MHz) source is broader than that of the low-frequency (2 MHz) source. In single-frequency CCPs, the influence of frequency on the power dissipation mode is different when the mode of the operating source is current or not. In current-driven CCPs, the ratio of ohmic heating to stochastic heating (P_{ohm}/P_{stoch}) is proportional to the square of frequency and the square of current density [8, 9]. In voltage-driven CCPs, the ratio of ohmic heating to stochastic heating (P_{ohm}/P_{stoch}) is proportional to the square root of voltage [9, 10]. Robiche *et al* presented the influence of current and frequency ratios on the sheath width and its voltage drop in current-driven dual-frequency CCPs [11]. Georgieva and Bogaerts presented the influence of voltage and frequency ratios on the IEDFs in voltage-driven dual-frequency CCPs, consisting of the high-frequency source of 27, 40, 60 or 100 MHz and the low-frequency source of 1 or 2 MHz [12]. They observed that the average ion energy is determined by the time-averaged sheath voltage affected by the voltage and frequency ratios. Kim *et al* suggested the effective parameters that can be analyzed for dual-frequency CCPs alike single-frequency CCPs [13]. When the high-frequency is much higher than the low-frequency, the ion flux and the ion energy distribution are dominantly controlled by the high-frequency and the low-frequency sources, respectively.

On the other hand, the plasma physics of triple-frequency capacitive discharges have not been fully understood as those of single-frequency and dual-frequency capacitive discharges [14]. The computer modeling can produce valuable diagnostics often not available experimentally and are more effective in time and cost less than experiments. The PIC-MCC models can describe the electron and ion kinetics in CCPs by solving the Newton–Lorentz and Maxwell equations for each particle [7, 12, 14–17]. The ion kinetics in a collisionless rf sheath are investigated by 1D PIC-MCC simulations of low-pressure (10 mTorr) argon plasmas sustained by triple-frequency (1, 30 and 120 MHz) source. Section 2 describes the simulation conditions for the capacitive coupled plasma reactor. Section 3 discusses the influence of current density (or voltage) and frequency ratios on the IEDFs at the driven electrode. The simulation results are compared with the analytical calculations of IEDFs in a collisionless rf sheath model through effective parameters (effective frequency, effective current and effective voltage) that can be analyzed for triple-frequency CCPs alike single-frequency CCPs.

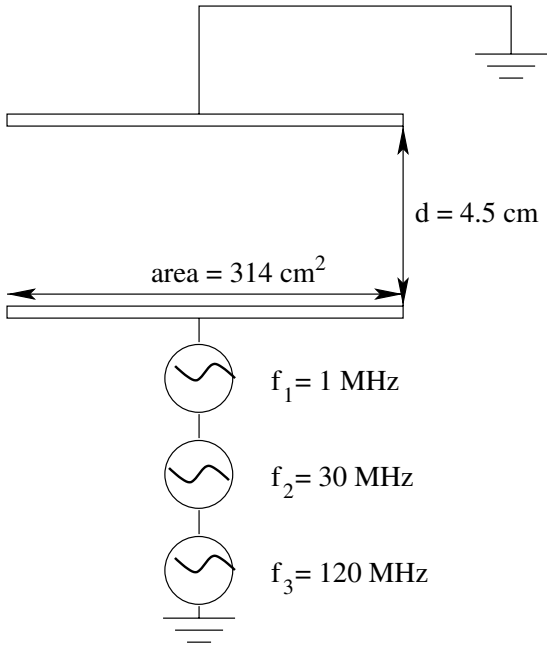

Figure 1. Schematic diagram of low-pressure (10 mTorr) argon plasmas sustained by the triple-frequency (1, 30 and 120 MHz) source in symmetrical current-driven and voltage-driven capacitively coupled plasma reactors.

2. Simulation conditions

We carried out 1D PIC-MCC simulations of low-pressure (10 mTorr) argon plasmas sustained by a triple-frequency (1, 30 and 120 MHz) source in symmetrical current-driven and voltage-driven capacitively coupled plasma reactors. For a pressure of 10 mTorr, the ion mean free path ranges from 0.3 to 0.75 cm for ions of 1–400 eV. If the ion mean free path is longer than the sheath length, the ion collisions such as charge exchange and elastic collisions in the sheath region can be neglected. The IEDFs on the driven electrode are determined by ions that cross the sheath region without undergoing ionic collisions such as charge exchange and elastic collisions. In simulations, the ion collisions in the sheath region are not considered. The sheath is defined as the region where the instantaneous electron density is less than half the instantaneous ion density and is updated at every time step.

Figure 1 shows the schematic diagram of low-pressure argon plasmas sustained by a triple-frequency source in symmetrical current-driven and voltage-driven capacitively coupled plasma reactors. The gap width between two electrodes is 4.5 cm and the area of electrodes is 314 cm^2. The gap width is divided into 800 cells, and the simulation time step is fixed to 4 ps to satisfy the simulation stability criteria and the Debye length. To satisfy the accuracy of PIC-MCC simulation, the number of superparticles per cell ranges from 100 to 200 because the statistical noise becomes inversely proportional to the number of superparticles.

3. Results and discussion

3.1. Analytic model for triple-frequency capacitive discharge

We describe the homogeneous plasma model for low-pressure (10 mTorr) and triple-frequency (1, 30 and 120 MHz) capacitive discharges under three assumptions. First, the total current density across the sheath is the sum of three current densities supplied to the triple-frequency source. From the first assumption, the operating rf current is expressed as

$$J_{\mathrm{rf}} = J_1 \cos(\omega_1 t) + J_2 \cos(\omega_2 t) + J_3 \cos(\omega_3 t), \tag{1}$$

where $f_1(=\omega_1/2\pi)$, $f_2(=\omega_2/2\pi)$ and $f_3(=\omega_3/2\pi)$ are the low frequency (1 MHz), the medium frequency (30 MHz) and the high frequency (120 MHz) of the triple-frequency source, respectively. J_1, J_2 and J_3 are the current densities of 1 MHz, 30 MHz and 120 MHz frequency sources, respectively.

Second, the instantaneous electron sheath edge is expressed as a step-like electron density profile at the time-varying electron sheath boundary, while ions have a time-independent and collisionless ion motion. From the second assumption, the net charge density $\rho(x,t)$, the instantaneous electric field $E(x,t)$ and the displacement current J_{d} are expressed as

$$\rho(x,t) = n, x < s(t), \tag{2a}$$

$$E(x,t) = \frac{en}{\epsilon_0}[x - s(t)], x < s(t), \tag{2b}$$

$$J_{\mathrm{d}} = -en\frac{\mathrm{d}s(t)}{\mathrm{d}t}, x < s(t), \tag{2c}$$

where n is the ion density and $s(t)$ is the sheath boundary.

Third, the current across the sheath is almost displacement current, i.e. the displacement current is much higher than the conduction current in the sheath region. From the third assumption, the sheath in triple-frequency capacitive discharges is expressed as

$$s(t) = \frac{J_1}{en\omega_1}[1 - \sin(\omega_1 t)] + \frac{J_2}{en\omega_2}[1 - \sin(\omega_2 t)] + \frac{J_3}{en\omega_3}[1 - \sin(\omega_3 t)], \tag{3a}$$

$$= \bar{s} - s_1 \sin(\omega_1 t) - s_2 \sin(\omega_2 t) - s_3 \sin(\omega_3 t). \tag{3b}$$

From equations (3*a*) and (3*b*), s_1, s_2, s_3 and the time-averaged sheath length $\bar{s}$ are expressed as

$$s_i = \frac{J_i}{en\omega_i}, i = 1, 2, 3, \tag{4a}$$

$$\bar{s} = \sum_{i=1}^{3} s_i. \tag{4b}$$

From equations (2*b*) and (3*b*), the voltages across the left-hand-side and the right-hand side sheaths are expressed as

$$V_{\mathrm{L}}(t) = \int_0^{s(t)} E\,\mathrm{d}x = -\frac{en}{\epsilon_0}\frac{s^2}{2}, \tag{5a}$$

$$= -\frac{en}{2\epsilon_0}\{s_1^2[1 - \sin(\omega_1 t)]^2 + s_2^2[1 - \sin(\omega_2 t)]^2 + s_3^2[1 - \sin(\omega_3 t)]^2 + 2s_1 s_2[1 - \sin(\omega_1 t)][1 - \sin(\omega_2 t)] + 2s_1 s_3[1 - \sin(\omega_1 t)][1 - \sin(\omega_3 t)] + 2s_2 s_3[1 - \sin(\omega_2 t)][1 - \sin(\omega_3 t)]\}. \tag{5b}$$

$$V_{\mathrm{R}}(t) = -\frac{en}{2\epsilon_0}\{s_1^2[1 + \sin(\omega_1 t)]^2 + s_2^2[1 + \sin(\omega_2 t)]^2 + s_3^2[1 + \sin(\omega_3 t)]^2 + 2s_1 s_2[1 + \sin(\omega_1 t)][1 + \sin(\omega_2 t)] + 2s_1 s_3[1 + \sin(\omega_1 t)][1 + \sin(\omega_3 t)] + 2s_2 s_3[1 + \sin(\omega_2 t)][1 + \sin(\omega_3 t)]\}. \tag{6}$$

From equations (5*b*) and (6), the time-averaged plasma potential $\bar{V}$ and the voltage $V(t)$ between the two electrodes are expressed as

$$\overline{V} = \int_0^T V_L(t)\,\mathrm{d}t = \frac{en}{\epsilon_0}\left[\frac{3}{4}(s_1^2 + s_2^2 + s_3^2) + s_1 s_2 + s_1 s_3 + s_2 s_3\right], \tag{7a}$$

$$V(t) = V_L(t) - V_R(t) = \frac{2en\bar{s}}{\epsilon_0}[s_1 \sin(\omega_1 t) + s_2 \sin(\omega_2 t) + s_3 \sin(\omega_3 t)] = V_1 \sin(\omega_1 t) + V_2 \sin(\omega_2 t) + V_3 \sin(\omega_3 t). \tag{7b}$$

From equation (7*b*), the amplitudes (V_1, V_2 and V_3) of the three frequency sources are given by

$$V_i = \frac{2en\bar{s}}{\epsilon_0}s_i, \qquad i = 1, 2, 3. \tag{8}$$

From equations (4*b*) and (8), the time-averaged plasma potential $\bar{V}$ can be expressed as a function of the amplitudes of the three frequency sources,

$$\overline{V} = \frac{3}{8}\left[(V_1 + V_2 + V_3) - \frac{2}{3}\left(\frac{V_1V_2 + V_2V_3 + V_3V_1}{V_1 + V_2 + V_3}\right)\right] = \frac{3}{8}V_{\mathrm{eff}}. \tag{9}$$

The effective voltage V_{eff} in the triple-frequency capacitive discharge can be derived as

$$V_{\mathrm{eff}} = (V_1 + V_2 + V_3) - \frac{2}{3}\left(\frac{V_1V_2 + V_2V_3 + V_3V_1}{V_1 + V_2 + V_3}\right). \tag{10}$$

Utilizing the expressions for the ohmic heating and stochastic heating powers of the single rf source [9], the time-averaged electron power $\overline{S_{\mathrm{e}}}$ in the triple-frequency capacitive discharge can be derived as

$$\overline{S_{\mathrm{e}}} = \frac{1}{2}\left(\frac{m\nu_{\mathrm{m}}d}{e^2n} + \frac{2m\overline{v_{\mathrm{e}}}}{e^2n}\right)(J_1^2 + J_2^2 + J_3^2), \tag{11}$$

where m and d are the electron density and the length of the bulk plasma, respectively; ν_{m} and $\overline{v_{\mathrm{e}}}$ are the electron–neutral collision frequency for momentum transfer and the mean electron speed, respectively.

Substituting the relation $\overline{S_{\mathrm{e}}} = (R_{\mathrm{eff}}J_{\mathrm{eff}}^2)/2$ in equation (11), the effective current density J_{eff} in the triple-frequency capacitive discharge can be derived as

$$J_{\mathrm{eff}} = (J_1^2 + J_2^2 + J_3^2)^{1/2}. \tag{12}$$

where R_{eff} is $(m\nu_{\mathrm{m}}d + 2m\overline{v_{\mathrm{e}}})/(e^2n)$. The time-averaged ion power $\overline{S_{\mathrm{i}}}$ of the single rf source is expressed as [9]

$$\overline{S_{\mathrm{i}}} = 2enu_{\mathrm{B}}\left(\bar{V} + \frac{T_e}{2}\right), \tag{13}$$

where u_B and T_e are the Bohm velocity and the electron temperature, respectively.

From equations (4*a*) and (7*a*), equation (13) is expressed as a function of the current densities and frequencies,

$$\overline{S_i} = \frac{3}{2}\frac{nu_B}{\epsilon_0}\left[\left(\frac{J_1}{\omega_1}\right)^2 + \left(\frac{J_2}{\omega_2}\right)^2 + \left(\frac{J_3}{\omega_3}\right)^2 + \frac{4}{3}\left(\frac{J_1J_2}{\omega_1\omega_2} + \frac{J_2J_3}{\omega_2\omega_3} + \frac{J_1J_3}{\omega_1\omega_3}\right)\right] + enu_BT_e, \quad (14a)$$

$$= \frac{3}{2}\frac{nu_B}{\epsilon_0}\left(\frac{J_{eff}}{\omega_{eff}}\right)^2 + enu_BT_e. \quad (14b)$$

From equations (12) and (14*a*), the effective frequency as a function of the current density and frequency ratios of the triple-frequency source can be derived as

$$\omega_{eff} = \omega_1\left[\left[1 + \left(\frac{J_2}{J_1}\right)^2 + \left(\frac{J_3}{J_1}\right)^2\right] \times \left[1 + \left(\frac{\omega_1}{\omega_2}\right)^2\left(\frac{J_2}{J_1}\right)^2 + \left(\frac{\omega_1}{\omega_3}\right)^2\left(\frac{J_3}{J_1}\right)^2 + \frac{4}{3}\left\{\left(\frac{\omega_1}{\omega_2}\right)\left(\frac{J_2}{J_1}\right) + \left(\frac{\omega_1}{\omega_3}\right)\left(\frac{J_3}{J_1}\right) + \left(\frac{\omega_1^2}{\omega_2\omega_3}\right)\left(\frac{J_2J_3}{J_1^2}\right)\right\}\right]^{-1}\right]^{1/2}. \quad (15)$$

Substituting the relation $\omega_1(V_1/J_1) = \omega_2(V_2/J_2) = \omega_3(V_3/J_3)$ in equation (15), the effective frequency as a function of the voltage and frequency ratios of the triple-frequency source can be derived as

$$\omega_{eff} = \omega_1\left[\left[1 + \left(\frac{\omega_2}{\omega_1}\right)^2\left(\frac{V_2}{V_1}\right)^2 + \left(\frac{\omega_3}{\omega_1}\right)^2\left(\frac{V_3}{V_1}\right)^2\right] \times \left[1 + \left(\frac{V_2}{V_1}\right)^2 + \left(\frac{V_3}{V_1}\right)^2 + \frac{4}{3}\left\{\left(\frac{V_2}{V_1}\right) + \left(\frac{V_3}{V_1}\right) + \left(\frac{V_2}{V_1}\right)\left(\frac{V_3}{V_1}\right)\right\}\right]^{-1}\right]^{1/2}. \quad (16)$$

Table 1 shows the effective frequency, the effective current density and the effective voltage calculated from equations (9), (12), (14*a*), (14*b*) and (15) exhibiting the current density or voltage ratio of the triple-frequency source. Figure 2(*a*) shows the effective frequency with respect to the current density ratio for the 1, 30 and 120 MHz sources. Figure 2(*b*) shows the effective frequency with respect to the voltage ratio for the 1, 30 and 120 MHz sources. The evolution of the effective frequency with the current density or voltage ratio of the three frequency sources is different depending on the mode of operating source, which is either voltage or current. The effective frequency in current-driven CCPs is dominantly controlled by the low-frequency source, when $J_3/J_1 \ll 1$ and $J_2/J_1 \ll 1$. On the other hand, the effective frequency in voltage-driven CCPs is not dominantly controlled by the low-frequency source, when $V_3/V_1 \ll 1$ and $V_2/V_1 \ll 1$. The effective frequency in voltage-driven CCPs is 2–10 times higher than that of current-driven CCPs at the same ratio of current density and voltage. The discharges in current-driven CCPs are not sustained under the conditions of $J_3/J_1 < 1.59$ and $J_2/J_1 < 2.5$. The discharges in voltage-driven CCPs are not sustained under the conditions of $V_3/V_1 < 0.075$ and $V_2/V_1 < 0.037$. The lowest effective frequency at which the discharges can be sustained is 2.5 MHz and 8 MHz for current-driven and voltage-driven CCPs, respectively. As a result, the current-driven CCPs are more desirable than the voltage-driven CCPs from the aspect of independent control of ion flux and ion bombardment energy because the ion energy width increases with decreasing effective frequency.

Table 1. Effective frequency (f_{eff}), effective current density (J_{eff}) and effective voltage (V_{eff}) with the current density or voltage ratio of the triple-frequency (1, 30 and 120 MHz) source.

1 MHz/30 MHz/120 MHz	f_{eff} (MHz)	J_{eff} (A m^{-2})	V_{eff} (V)
0.0628 A/0.157 A/0 A	2.5	5.4	
0.0628 A/0.942 A/0.785 A	13.4	39.1	
0.0628 A/0.942 A/3 A	30	100.2	
270 V/10 V/20 V	8		318.4
150 V/100 V/50 V	25		361.1
100 V/100 V/100 V	46		366.7
50 V/100 V/150 V	68		361.1
10 V/10 V/280 V	114		312.7

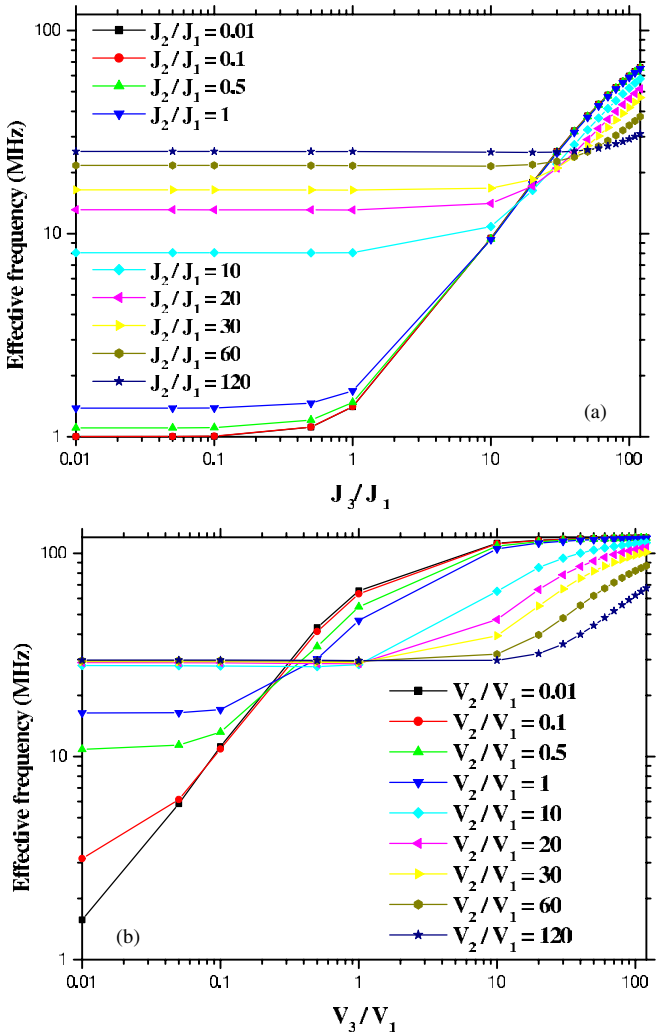

Figure 2. (*a*) Effective frequency with respect to the current density ratio of the triple-frequency source; (*b*) effective frequency with respect to the voltage ratio of the triple-frequency source.

Table 2. Time-averaged sheath potential ($\overline{V_s}$), time-averaged sheath length ($\bar{s}$), time-averaged electron density ($\overline{N_e}$) and time-averaged electron temperature ($\overline{T_e}$) with respect to the current or voltage ratio of the triple-frequency (1, 30 and 120 MHz) source.

1 MHz/30 MHz/120 MHz	$\overline{V_s}(V)$	$\bar{s}$(cm)	$\overline{N_e}(m^{-3})$	$\overline{T_e}$(eV)
0.0628 A/0.157 A/0 A	290	1.75	1.7×10^{15}	0.42
0.0628 A/0.942 A/0.785 A	120	0.6	3.8×10^{15}	2.08
0.0628 A/0.942 A/3 A	85	0.3	5.4×10^{15}	2.33
270 V/10 V/20 V	115	0.75	2.2×10^{15}	1.91
150 V/100 V/50 V	105	0.5	7.0×10^{15}	1.95
100 V/100 V/100 V	109	0.45	1.0×10^{16}	2.50
50 V/100 V/150 V	113	0.36	2.5×10^{16}	2.25
10 V/10 V/280 V	115	0.19	7.3×10^{16}	2.15

3.2. 1D PIC-MCC simulations with ion-collisionless sheath model

Table 2 shows the plasma characteristics calculated from the 1D PIC-MCC simulation with respect to the current or voltage ratio of the triple-frequency source. The rf discharge parameters such as the time-averaged plasma potential, the time-averaged sheath length and the time-averaged powers dissipated by electrons and ions can be expressed as the effective frequency and the effective current density (or the effective voltage). The time-averaged plasma potential is $(3/8)V_{\text{eff}}$. The time-averaged sheath length is proportional to the sum of the ratio of current density to the frequency of the three frequency sources. The time-averaged electron power is proportional to the square of the effective current density, and the time-averaged ion power is proportional to the square of the ratio of effective current density to effective frequency. Figure 3(a) shows the time-averaged plasma potential profile at different current ratios of the triple-frequency source. As the current ratio of the high-frequency (120 MHz) source increases, the time-averaged sheath potential decreases due to the increase in the ratio of time-averaged electron power to time-averaged ion power. The electron temperature also increases due to the increase in the ratio of time-averaged electron power to time-averaged ion power with increasing current ratio of the high-frequency (120 MHz) source, as shown in table 2. Figure 3(b) shows the time-averaged plasma potential profile at different voltage ratios of the triple-frequency source. As the voltage ratio of the high-frequency (120 MHz) source increases, the time-averaged sheath potential and electron temperature do not much change because the ratio of ohmic heating to stochastic heating in single-frequency voltage-driven CCPs is proportional to the square root of voltage [9, 10].

Figure 4(a) shows the IEDFs with respect to the current ratio of triple-frequency source. The IEDFs on the driven electrode are affected by the ratio of the ion transit time ($\tau_{\text{ion}} = 3\bar{s}(M/2e\overline{V_s})^{1/2}$) to the rf period ($\tau_{\text{rf}} = 2\pi/w_{\text{eff}}$), which is expressed as a function of the effective frequency, the sheath length and the mean potential difference between the driven electrode and the plasma, where M is the argon ion mass (6.68×10^{-26} kg) and e is the electron charge (1.602×10^{-19} C). The ion transit time can be calculated from the time-averaged sheath voltage and the time-averaged sheath length in table 2 .

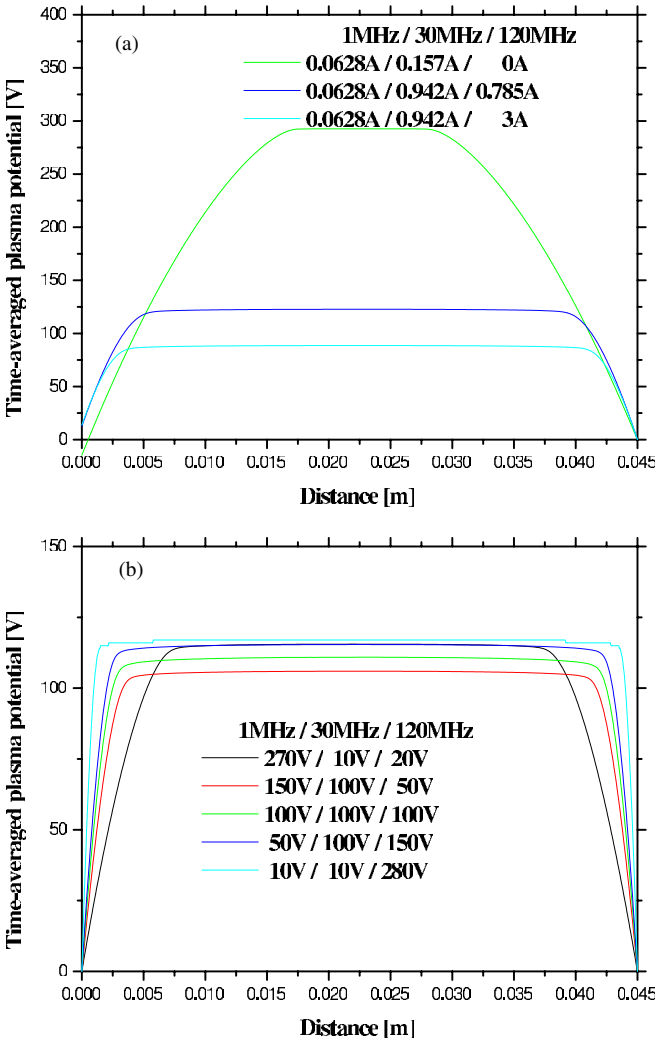

Figure 3. (a) Time-averaged plasma potential profile with the current ratio of the triple-frequency (1, 30 and 120 MHz) source; (b) time-averaged plasma potential profile with the voltage ratio of the triple-frequency (1, 30 and 120 MHz) source.

The rf period with respect to the current or voltage ratio of the triple-frequency source should be substituted for the effective frequency in table 1. In the case of 0.0628 A (1 MHz)/0.157 A (30 MHz)/0 A (120 MHz), the ion transit time and the rf period are 1.408 μs and 0.4 μs, respectively. The ratio of the ion transit time to the rf period is 3.52. In the case of 0.0628 A (1 MHz)/0.942 A (30 MHz)/0.785 A (120 MHz), the ion transit time and the rf period are 0.75 μs and 0.074 μs, respectively. The ratio of the ion transit time to the rf period is 10.14. In the case of 0.0628 A (1 MHz)/0.942 A (30 MHz)/3 A (120 MHz), the ion transit time and the rf period are 0.456 μs and 0.033 μs, respectively. The ratio of the ion transit time to the rf period is 13.52. In the regime of $\tau_{\text{ion}}/\tau_{\text{rf}} \gg 1$, ions respond to the time-averaged sheath voltage because ions cross the sheath in a time corresponding to many rf cycles. The average ion energy on IEDFs decreases due to the reduction in the time-averaged sheath voltage caused by the transition of the power dissipation mode with increasing current ratio of the high-frequency source. As the current ratio of the high-frequency source increases, the width of IEDFs decreases due to the

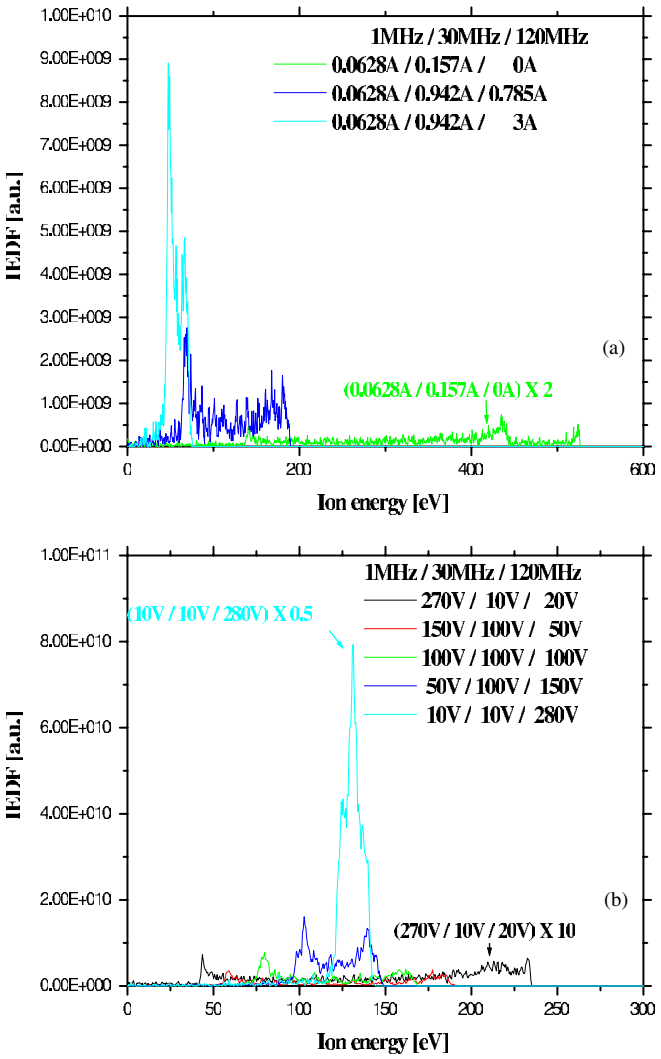

Figure 4. (*a*) Effective frequency with respect to the current density ratio of the triple-frequency source; (*b*) effective frequency with respect to the voltage ratio of the triple-frequency source.

reduction in the time-averaged sheath voltage (cf table 2) as well as the increase in the effective frequency (cf table 1).

Figure 4(*b*) shows the IEDFs with respect to the voltage ratio of the triple-frequency source. The ion transit time and the rf period are 0.958 μs and 0.125 μs, 0.668 μs and 0.04 μs, 0.59 μs and 0.021 μs, 0.464 μs and 0.014 μs and 0.242 μs and 0.008 μs for voltages of high-frequency source of 20 V, 50 V, 100 V, 150 V and 280 V, respectively. The ratio of the ion transit time to the rf period is 7.67, 16.7, 28.1, 33.1 and 30.3 for voltages of the high-frequency source of 20 V, 50 V, 100 V, 150 V and 280 V, respectively. Ions respond to the time-averaged sheath voltage. The average ion energy on IEDFs remains unaltered with increasing voltage of the high-frequency source. The width of IEDFs, however, decreases due to the increase in the effective frequency, even with the decrease in the sheath length.

The sheath voltage and the analytical IEDF in the high-frequency ($\tau_{\rm ion}/\tau_{\rm rf} \gg 1$) regime, assuming a constant sheath width, a uniform sheath electric field, a sinusoidal sheath voltage and zero initial ion velocity at the plasma-sheath boundary, are expressed as [3]

$$V_{\rm s}(x,t) = V_{\rm s}(t)(x/s)^{4/3} = \overline{V_{\rm s}}[1+\lambda\sin(\omega_{\rm rf}t)](x/s)^{4/3}, \tag{17a}$$

$$f(E) = \frac{2\Gamma}{\omega_{\rm rf}\Delta E}\left[1-\left(\frac{2}{\Delta E}\right)^2(E-e\overline{V_{\rm s}})^2\right]^{-1/2}, \tag{17b}$$

where $\Delta E = (8\lambda e\overline{V_{\rm s}}/3\omega_{\rm rf}\bar{s})(2e\overline{V_{\rm s}}/M)^{1/2}$. λ is a parameter ($\lambda \leqslant 1$).

Figure 5 shows the sheath voltage profile over one period of 1 MHz calculated from the 1D PIC-MCC simulation with the voltage ratio of the triple-frequency source. As the voltage ratio of the high-frequency source decreases, the sheath voltage changes from a sinusoidal to a half-wave rectified type. The IEDF analytically calculated in the high-frequency ($\tau_{\rm ion}/\tau_{\rm rf} \gg 1$) regime by Goedheer *et al* is in contradiction to the assumption of a sinusoidal sheath voltage. In order to avoid this contradiction for the sheath voltage in triple-frequency CCPs, the expression of the sheath voltage is modified as

$$\begin{aligned} V_{\rm s}(x,t) &= V_{\rm s}(t)(x/s)^{4/3} \\ &= \overline{V_{\rm s}}[1+\lambda_1\sin(\omega_1 t)][1+\lambda_2\sin(\omega_2 t)] \\ &\quad\times[1+\lambda_3\sin(\omega_3 t)](x/s)^{4/3}, \end{aligned} \tag{18}$$

where λ_1, λ_2 and λ_3 are parameters ($\lambda_1, \lambda_2, \lambda_3 \leqslant 1$). The parameters ($\lambda_1$, λ_2 and λ_3) are determined by matching the sheath voltage in equation (18) to the sheath voltage calculated from the 1D PIC-MCC simulation in figure 5. The ion motion equation in sheath region is expressed as follows,

$$\begin{aligned} \frac{{\rm d}^2x}{{\rm d}t^2} &= \frac{4}{3}\left(\frac{e\overline{V_{\rm s}}}{Ms}\right)[1+\lambda_1\sin(\omega_1 t)][1+\lambda_2\sin(\omega_2 t)] \\ &\quad\times[1+\lambda_3\sin(\omega_3 t)](x/s)^{1/3}. \end{aligned} \tag{19}$$

If the ion transit time is much higher than the rf period, the ion path corresponds to the average acceleration as

$$x(t) = s\left[\frac{1}{3s}\left(\frac{e\overline{V_{\rm s}}}{M}\right)^{1/2}\right]^3(t-t_0)^3, \tag{20}$$

where t_0 is the time at which the ion enters the sheath region.

The substitution of equation (20) into equation (19) gives

$$\begin{aligned} \frac{{\rm d}^2x}{{\rm d}t^2} &= \frac{2}{9s^2}\left(\frac{2e\overline{V_{\rm s}}}{M}\right)^{\frac{3}{2}}[1+\lambda_1\sin(\omega_1 t)][1+\lambda_2\sin(\omega_2 t)] \\ &\quad\times[1+\lambda_3\sin(\omega_3 t)](t-t_0). \end{aligned} \tag{21}$$

The time integration of equation (21) yields the velocity

$$\begin{aligned} \frac{{\rm d}x}{{\rm d}t} \approx \frac{2}{9s^2}\left(\frac{e\overline{V_{\rm s}}}{Ms}\right)^{3/2}\Bigg[&\frac{1}{2}(t-t_0)^2 - \frac{\lambda_1}{\omega_1}(t-t_0)\cos(\omega_1 t) \\ &-\frac{\lambda_2}{\omega_2}(t-t_0)\cos(\omega_2 t) - \frac{\lambda_3}{\omega_3}(t-t_0)\cos(\omega_3 t)\Bigg]. \end{aligned} \tag{22}$$

From equation (20), the time interval in which the ions cross the sheath is given by

$$(t_1 - t_0) = 3s\left(\frac{M}{2e\overline{V_{\rm s}}}\right)^{1/2}. \tag{23}$$

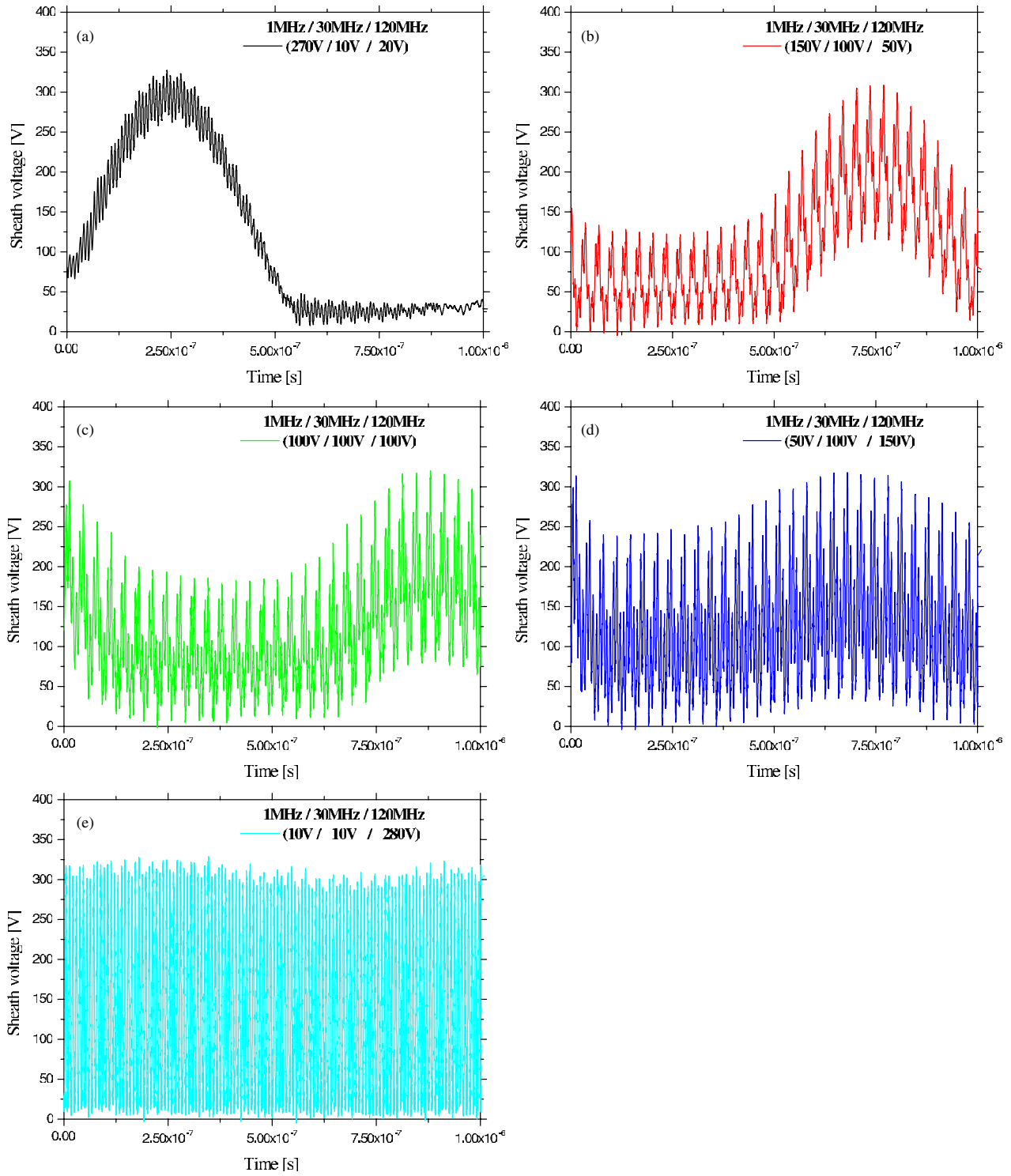

Figure 5. Sheath voltage profile over one period of 1 MHz calculated from the 1D PIC-MCC simulation with the voltage ratio of the triple-frequency (1, 30 and 120 MHz) source. (*a*) 270 V/10 V/20 V; (*b*) 150 V/100 V/50 V; (*c*) 100 V/100 V/100 V; (*d*) 50 V/100 V/150 V; (*e*) 10 V/10 V/280 V.

From equations (21) and (22), the ion energy at the electrode is given by

$$E = e\overline{V_s}\left[1 - \frac{2}{3s}\left(\frac{2e\overline{V_s}}{M}\right)^{1/2}\left[\frac{\lambda_1}{\omega_1}\cos(\omega_1 t) + \frac{\lambda_2}{\omega_2}\cos(\omega_2 t) + \frac{\lambda_3}{\omega_3}\cos(\omega_3 t)\right]\right]^2. \quad (24)$$

As a result, the IEDF and the ion energy width in triple-frequency CCPs are expressed as

$$f(E) = \frac{2\Gamma}{\omega_{\text{eff}}\Delta E}\left[1 - \left(\frac{2}{\Delta E}\right)^2 (E - e\overline{V_s})^2\right]^{-1/2}, \quad (25a)$$

$$\Delta E = \frac{8e\overline{V_s}}{3s}\left(\frac{2e\overline{V_s}}{M}\right)^{1/2}\left(\frac{\lambda_1}{\omega_1} + \frac{\lambda_2}{\omega_2} + \frac{\lambda_3}{\omega_3}\right). \quad (25b)$$

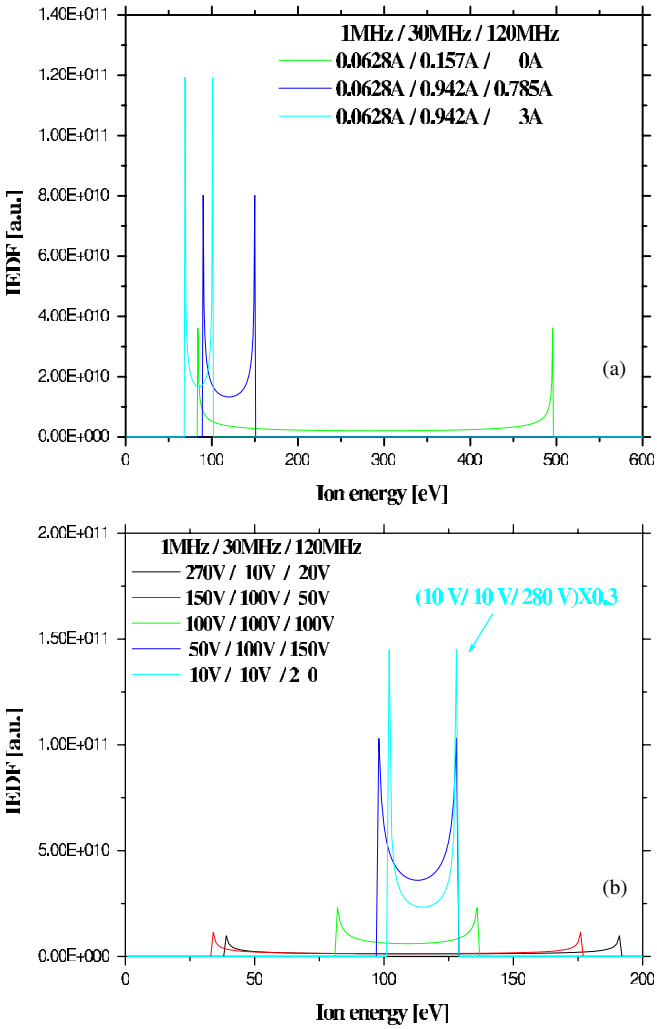

Figure 6. Analytical calculations of IEDFs in a collisionless rf sheath model through the effective frequency. (*a*) IEDFs with respect to the current ratio; (*b*) IEDFs with respect to the voltage ratio.

Figure 6 shows the analytical calculations of IEDFs in a collisionless rf sheath through the effective frequency (cf table 1) and the plasma characteristics calculated from the 1D PIC-MCC simulation (cf table 2). Figure 6(*a*) shows the analytical calculations of IEDFs with respect to the current ratio of the triple-frequency source. As the current of the high-frequency source increases, the ion energy width decreases due to the reduction in the sheath potential as well as the increase in the effective frequency, even with the decrease in the sheath length. Figure 6(*b*) shows the analytical calculations of IEDFs with respect to the voltage ratio of the triple-frequency source. The width of IEDFs decreases due to the increase in the effective frequency, even with the decrease in the sheath length. In the case of 270 V (1 MHz)/10 V (30 MHz)/20 V (120 MHz), λ_1, λ_2 and λ_3 are 1, 0.1 and 0.01, respectively. In the case of 150 V (1 MHz)/100 V (30 MHz)/50 V (120 MHz), λ_1, λ_2 and λ_3 are 0.7, 0.4 and 0.3, respectively. In the case of 100 V (1 MHz)/100 V (30 MHz)/100 V (120 MHz), λ_1, λ_2 and λ_3 are 0.5, 0.4 and 0.7, respectively. In the case of 50 V (1 MHz)/100 V (30 MHz)/150 V (120 MHz), λ_1, λ_2 and λ_3 are 0.005, 0.4 and 0.9, respectively. In the case of 10 V (1 MHz)/10 V (30 MHz)/280 V (120 MHz), λ_1, λ_2 and λ_3 are 0.001, 0.05 and 1, respectively. The ion energy width is determined by the ratio of the sheath voltage to the frequency of the three frequency sources, not the low-frequency (1 MHz) source. The ion energy width calculated from equations (25*a*) and (25*b*) is 152 eV, 142 eV, 54 eV, 30 eV and 26 eV for the voltages of high-frequency source of 20 V, 50 V, 100 V, 150 V and 280 V, respectively. The ion energy width calculated from PIC-MCC simulation is 192 eV, 134 eV, 80 eV, 53 eV and 25 eV for voltages of the high-frequency source of 20 V, 50 V, 100 V, 150 V and 280 V, respectively. In the case of 270 V (1 MHz)/10 V (30 MHz)/20 V (120 MHz), the large difference (40 eV) in the ion energy width calculated from analytic and PIC-MCC models exists due to the aberration of λ_1, λ_2 and λ_3 caused by a half-wave rectified type of the sheath voltage. These analytical results of IEDFs in a collisionless rf sheath model through the effective frequency are in qualitative agreement with the PIC-MCC simulation results. The ion energy width of the IEDF is controlled by the effective frequency, which is expressed as a function of the voltage and frequency ratios of the triple-frequency source.

4. Conclusions

One-dimensional PIC-MCC simulations of low-pressure (10 mTorr) argon plasmas sustained by a triple-frequency (1, 30 and 120 MHz) source in symmetrical current-driven and voltage-driven capacitively coupled plasma reactors are presented. We conclude that the effective current, the effective voltage and the effective frequency are helpful in explaining the physics of triple-frequency CCPs alike single-frequency CCPs. The rf discharge parameters such as the IEDF, the sheath length, the plasma potential and the powers dissipated by electrons and ions can be expressed as the effective frequency and the effective current density (or effective voltage). An analytic model of the IEDF for the triple-frequency CCPs in the high-frequency regime is developed. The analytical calculations of the IEDF in the high-frequency regime through the effective frequency visualized in this paper are in qualitative agreement with the simulation results of the IEDF calculated from the 1D PIC-MCC model. The ion energy width and average ion energy of IEDF are controlled by the effective frequency, which is expressed as a function of the current density (or voltage) and frequency ratios of the triple-frequency source. The evolution of the effective frequency with the current density or voltage ratio of the three frequency sources is different depending on the mode of operating source, which is either voltage or current. The effective frequency in voltage-driven CCPs is 2–10 times higher than that of current-driven CCPs at the same ratio of current density and voltage. As a result, the current-driven CCPs are more desirable than the voltage-driven CCPs from the aspect of independent control of ion flux and ion bombardment energy because the ion energy width increases with decreasing effective frequency.

Acknowledgments

This work was supported by the Commercialization Program of Nano Process Equipment program, the Korea Science

and Engineering Foundation (KOSEF) grant funded by the Korea government (MOST) (No R01-2007-000-10730-0) and the Korea Ministry of Education through its Brain Korea 21 program.

References

[1] Kawamura E, Vahedi V, Lieberman M A and Birdsall C K 1999 *Plasma Sources Sci. Technol.* **8** R45
[2] Benoit-Cattin P and Bernard L C 1968 *J. Appl. Phys.* **39** 5723
[3] Goedheer W J 2000 *Plasma Sources Sci. Technol.* **9** 507
[4] Wild C and Koidl P 1989 *Appl. Phys. Lett.* **54** 505
[5] May P W, Field D and Kelmperer D F 1992 *J. Appl. Phys.* **71** 3721
[6] Manuilenko O V, Babaeva N Y, Kim H C, Lee J K and Shon J W 2005 *Plasma Sources Sci. Technol.* **14** 89
[7] Georgieva V, Bogaerts A and Gijbels R 2004 *Phys. Rev.* E **69** 026406
[8] You S J, Ahn S K and Chang H Y 2006 *Appl. Phys. Lett.* **89** 171502
[9] Lieberman M A and Lichtenberg A J 2005 *Principles of Plasma Discharges and Materials Processing* 2nd edn (New York: Wiley)
[10] Abdel-Fattch E and Sugai H 2003 *Appl. Phys. Lett.* **83** 1533
[11] Robiche J, Boyle P C, Turner M M and Ellingboe A R 2003 *J. Phys. D: Appl. Phys.* **36** 1810
[12] Georgieva V and Bogaerts A 2005 *J. Appl. Phys.* **98** 023308
[13] Kim H C, Lee J K and Shon J W 2003 *Phys. Plasmas* **10** 4545
[14] Alan Wu C F, Lieberman M A and Verboncoeur J P 2007 *J. Appl. Phys.* **101** 056105
[15] Kim H C and Lee J K 2004 *Phys. Rev. Lett.* **93** 085003
[16] Kim H C, Iza F, Yang S S, Radmilovic-Radjenovic M and Lee J K 2005 *J. Phys. D: Appl. Phys.* **36** R 283–301
[17] Park G Y, You S J, Iza F and Lee J K 2007 *Phys. Rev. Lett.* **98** 085003